WATER RESOURCES RESEARCH, VOL. 32, NO. 7, PAGES 1943–1954, JULY 1996

# Influence of specific surface area on transport of sorbing solutes in fractures: An experimental analysis

Christoph Wels[1] and Leslie Smith

Geological Engineering Program, Department of Earth and Ocean Sciences, University of British Columbia, Vancouver, British Columbia, Canada

T. T. Vandergraaf

Whiteshell Laboratories, Atomic Energy of Canada Limited, Pinawa, Manitoba, Canada

**Abstract.** Experimental evidence is presented on the influence of specific surface area on the transport of the sorbing tracer strontium in fractures with uniform, but differing aperture. Specific surface area is defined as the ratio of the fracture surface area to the volume of mobile water in the fracture. Static sorption experiments on granite coupons suggest hysteresis in the sorption process, showing higher surface distribution coefficients for desorption than for sorption. Strontium was subject to significantly greater dispersion than the nonreactive tracer tritium. This enhanced dispersion is believed to be the result of chemical heterogeneity at the mineral grain scale, hysteresis in sorption, and limited transverse mixing across the fracture aperture. The influence of fracture aperture on retardation is much greater than predicted by the commonly used definition of the surface retardation factor. Strontium retardation was approximately an order of magnitude greater in a smaller-aperture fracture (450 $\mu$m, $R_a \sim 45$) than in a large-aperture fracture (780 $\mu$m, $R_a \sim 3.5$). We hypothesize that hysteresis in sorption, in conjunction with limited transverse mixing across the aperture, caused the apparent increase in sorption strength ($K_a$) with a decrease in fracture aperture.

## Introduction

During transport within a low-permeability fractured medium, solutes may sorb either directly to fracture walls (surface sorption), or they may diffuse into the porous matrix where they sorb on intragranular and intergranular surfaces (matrix sorption). Both processes lead to delayed arrival of solutes at a downstream boundary and can cause strong tailing in the breakthrough curve. The extent of both surface sorption and diffusive transfer to the matrix depends on the specific surface area of a fracture. Specific surface area is defined as the ratio of the fracture surface area to the volume of mobile water in the fracture. Model studies suggest that the magnitude of the specific surface area can have a strong impact on retardation of a solute plume [*Moreno and Neretnieks*, 1993]. *Wels and Smith* [1994] further suggested that the link between retardation and specific surface area at the scale of a single fracture produces nonuniform and anisotropic retardation of the plume at the network scale. In this paper we present experimental evidence on the influence of specific surface area on the transport of the sorbing tracer strontium in fractures with uniform, but differing aperture.

Surprisingly few experimental studies have been reported that document the processes controlling reactive solute transport in single fractures. Neretnieks and coworkers carried out migration experiments using strontium and cesium in natural, rough-walled fractures in granite [*Neretnieks et al.*, 1982; *Moreno et al.*, 1985]. Interpretation of the breakthrough curves was complicated by the rough walls of the fracture and the consequent dispersion that occurred because of channeling. *Neretnieks et al.* [1982] modeled the dispersion process assuming the solute traveled in a set of independent, parallel channels with different channel apertures. They found that the advective movement of a sorbing tracer displayed a stronger dependence on channel aperture than did a nonreacting tracer (tracer velocity proportional to aperture cubed versus aperture squared, respectively). In a follow-up experiment, *Moreno et al.* [1985] demonstrated that either an advection-dispersion model or their channel model could fit the experimental breakthrough curves. However, the choice of a particular dispersion model influenced the estimated values of the parameters describing surface sorption and matrix diffusion/sorption.

The interpretation of reactive transport experiments is further complicated when chemical heterogeneity is present or the solute exhibits nonideal sorption behavior [e.g., *Vandergraaf*, 1995; *Vandergraaf et al.*, 1994]. Both factors can enhance dispersion relative to that experienced by a nonreactive tracer. Chemical heterogeneity is usually defined as spatial heterogeneity in sorption sites and/or sorption strength of the sorbing material. Nonideal sorption behavior includes (1) nonlinear sorption, (2) chemical nonequilibrium, and (3) hysteresis in sorption. *Neretnieks et al.* [1982] suggested that the nonlinear nature of the cesium isotherm could have caused the discrepancies they observed between peak outflow concentrations and model predictions based on a linear sorption model. Hysteresis between adsorption and desorption is frequently observed, in particular for strongly bound ions, with desorption taking more time to attain equilibrium than adsorption [*Davis and Kent*, 1990].

[1]Now at Robertson Geoconsultants, Inc., Vancouver, British Columbia, Canada.



Paper number 96WR00895.
0043-1397/96/96WR-00895$09.00

The influence of chemical heterogeneity and nonideal sorption on dispersion in fractures is probably best examined in a fracture with uniform aperture. In this case, Taylor dispersion is the only physical mechanism that spreads mass along the fracture. Dispersion of conservative and ideally sorbing solutes in a constant-aperture fracture has been described using analytical techniques [*Kessler and Hunt*, 1994], numerical simulations [*Wels*, 1995], and migration experiments [*Vandergraaf et al.*, 1988; *Fujikawa et al.*, 1993]. *Vandergraaf et al.* [1988] noted that for a continuous injection of tracer into a sawed fracture in granite, dispersion of cesium was considerably greater than that for a conservative tracer. They suggested that deviations from the linearity and reversibility of the sorption process could have resulted in front sharpening or tailing of the elution profile. A quantitative analysis of the breakthrough curves was not presented. *Fujikawa et al.* [1993] performed migration experiments similar to those of *Vandergraaf et al.* [1988], using pulse injections of cesium. They noted a strong dependence of the breakthrough curves, in particular peak height and tailing, on the fluid velocity in the fracture. A transport model that accounted for surface sorption and matrix diffusion/sorption was fit to the experimental data. They found that the parameters characterizing the sorption process had to be varied significantly to obtain a good fit for the experiments with different fluid velocities. The authors proposed that microscopic heterogeneities in the diffusion/sorption potential of the rock matrix could be responsible for the discrepancies in parameter estimates. They noted that a consideration of nonlinear sorption may have improved the model fit. The possibility of nonequilibrium sorption and/or hysteresis in sorption was not considered.

None of these experimental studies have focused on the influence of specific surface area on transport. To illustrate the influence of specific surface area $a_w$ consider the transport of a sorbing solute in a single fracture. In a smooth, constant aperture fracture, the specific surface area is equal to 2 times the inverse of the fracture aperture (i.e., $a_w = 2/b$). Assuming fast, linear, and reversible sorption, the equation describing solute transport in the fracture is [e.g., *Moreno et al.*, 1985]:

$$R_a \frac{\partial C_f}{\partial t} = D_L \frac{\partial^2 C_f}{\partial x^2} - u \frac{\partial C_f}{\partial x} + a_w D_e \left.\frac{\partial C_p}{\partial z}\right|_{z=0} \quad (1)$$

where $D_e$ is the effective diffusion coefficient for the matrix, defined by *Neretnieks* [1980] as ($D_e = \varepsilon_p \tau D_m$), and $R_a$ is the surface retardation factor, defined as

$$R_a = 1 + a_w K_a \quad (2)$$

All the parameters are defined in the notation list. Assuming only diffusive mass transfer in the porous matrix, solute movement is described by

$$\frac{\partial C_p}{\partial t} = \frac{D_e}{K_v} \frac{\partial^2 C_p}{\partial z^2} \quad (3)$$

where $K_v$ is related to the sorption capacity of the rock $K_D \rho_s$ by [*Neretnieks*, 1980]

$$K_v = \varepsilon_p + K_D \rho_s \quad (4)$$

where $K_D$ is the bulk distribution coefficient. Note that *Moreno and Neretnieks* [1993] refer to $a_w$ as the "flow-wetted surface" of a fracture. We prefer the use of "specific surface area" indicating that $a_w$ is the ratio of the fracture surface area to the fracture volume with units $m^2/m^3$.

The specific surface area $a_w$ influences solute transport in two ways. First, $a_w$ enters into the definition of the surface retardation factor (equation (2)). A larger $a_w$ implies a greater surface area for surface sorption to take place relative to the amount of tracer in solution. As a result, a greater amount of tracer is sorbed, the surface retardation factor increases, and the solute plume in the fracture advances at a slower rate. Second, the specific surface area also influences the fourth term in (1), which describes the rate of exchange of the solute with the matrix. This term implies that a larger specific surface area provides more access of the solute to diffuse from the open fracture into the rock matrix relative to the amount of tracer in solution. Therefore a sorbing solute traveling in a fracture with a high specific surface area (i.e., a narrow aperture) should experience more retardation and more tailing than the same solute traveling in a wider fracture, assuming rock properties are the same.

In this paper we report migration experiments using machined fractures which differ only in fracture aperture. The simple geometry of the fracture permits an interpretation of experimental breakthrough curves by means of the transport model (1)–(4). The surface and bulk distribution coefficients $K_a$ and $K_D$ are estimated independently from static sorption experiments. The experimental results presented here demonstrate that the influence of specific surface area on solute retardation may be of significantly greater magnitude than predicted by the surface retardation factor (2).

## Materials and Methods

### Migration Experiments

The migration experiments were performed in rectangular, constant-aperture fractures. The fractures were constructed by joining two slabs of granite with dimensions $10.0 \times 2.5 \times 1.25$ $cm^3$ each. The granite slabs were cut from quarried blocks of the Lac du Bonnet Batholith, Manitoba, Canada [*Vandergraaf et al.*, 1982]. The fractures were made by placing narrow Teflon spacers of desired thickness (i.e., aperture) between two granite slabs. The surfaces of the slabs facing the fracture were polished to minimize the roughness of the fracture walls. The slabs were saturated with distilled water prior to mounting, and the outer surfaces of the mounted slabs were sealed with silicone rubber to avoid evaporation from the rock matrix. The granite slabs were then mounted to inflow/outflow plenums (see below) using silicone rubber as a glue and sealant. Prior to each experiment, distilled water was circulated through the experimental apparatus for 24 hours at a rate similar to that used in each experiment.

The use of polished fracture surfaces simplifies the interpretation of breakthrough curves for fractures with different aperture. The polishing of the fracture surface may, however, both influence the sorptive properties of the fracture surface and clog microcracks which form the primary porosity of the granite. Because each slab was polished in the same manner, and our focus here is on the change in surface retardation due to differences in specific surface area, rather than on its absolute magnitude, there are distinct advantages to using polished fracture surfaces.

Two experimental setups were used in the migration experiments which are shown in Figures 1a and 1b. For a continuous or step input of tracer, solutions tagged with radionuclides

were passed through the fracture using a gravity feed system (Figure 1a). A Teflon reservoir ($5 \times 5 \times 5$ cm$^3$) was mounted directly on top of the joined slabs, allowing the solution to enter the open fracture directly through a narrow slit ($2.2 \times 0.1$ cm$^2$) in the base of the reservoir. The outflow from the fracture was funneled via a triangular slit (cut to 1 mm depth) in a Teflon plenum into narrow Teflon tubing (ID = 0.025 cm). A tubing length of 0.9 m provided sufficient resistance to obtain the desired flow rates. The background solution in the inflow reservoir could be manually replaced by tracer solution or vice versa in a short time period (<2 min). For a pulse injection, tracer solution was delivered using a high-pressure liquid chromatography (HPLC) pump (Figure 1b). In this setup, both ends of the joined slabs were mounted directly to Teflon plenums which were connected to inflow and outflow tubing. For injection of the tracer solution the flow pump was stopped, and valves 1 and 2 were switched from position "1" to position "0." The tracer solution was then injected with a syringe into the tubing between valves 1 and 2 (Figure 1b). The volume of tracer solution injected was sufficient to displace all distilled water in the tubing which was pushed out past valve 1 into the overflow tubing (Figure 1b). Then valves 1 and 2 were switched back to the original position "1," and the flow pump started again to allow flow of the tracer slug (~0.5 mL) into the mounted fracture. In both setups the outflow from the core was collected with a fraction collector which was set to collect 2 drops per vial for the tritium breakthrough and between 4 and 12 drops per vial for the strontium breakthrough. The drop volume, repeatedly determined by weighing spot samples, was of the order of 0.05 ml (±10%). The sample drops were collected directly in scintillation vials (prefilled with Insta-gel®) which were subsequently analyzed for the radioactive tracers (Sr-90/$^3H_2O$) using liquid scintillation counting. This procedure minimized potential errors caused by evaporation and sample transfer of these small sample volumes.

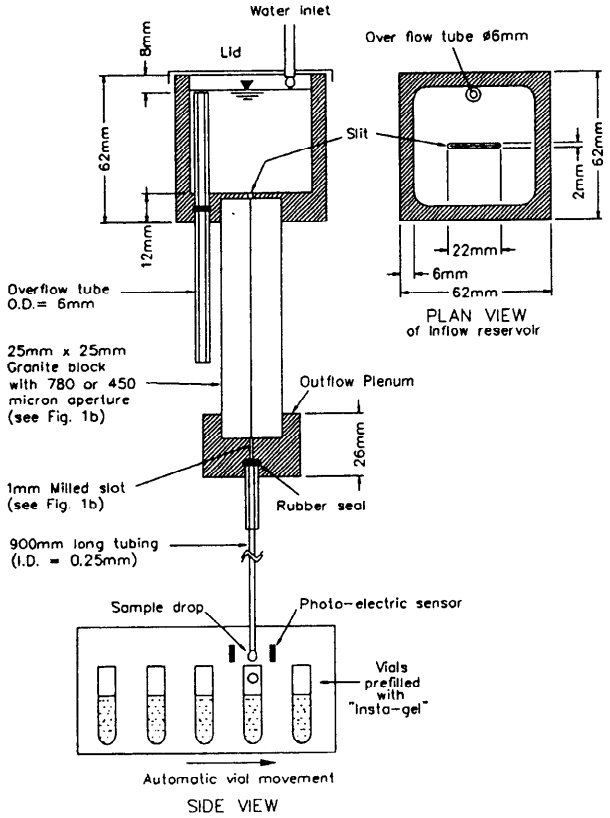


**Figure 1a.** Experimental setup for migration experiments using finite step injection.

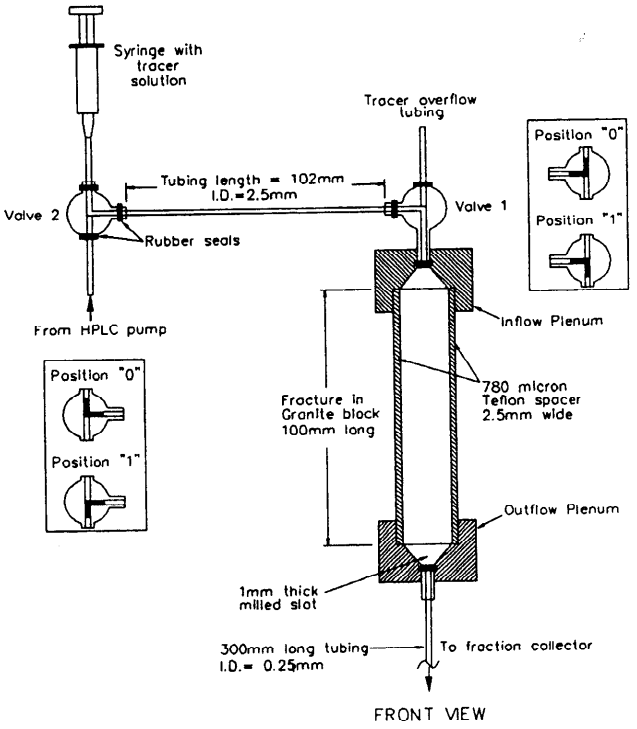


**Figure 1b.** Experimental setup for migration experiments using pulse injection.

Three migration experiments were performed (Table 1). To study the effect of specific surface area, migration experiments were run in a large-aperture and smaller-aperture fracture. The experiments also differed with respect to the injection scheme. In experiment 1 the tracer solution was injected as a short pulse (duration of the injection, $\Delta t$ = 0.35 hour). In experiments 2 and 3 the tracer solution was injected as a step input ($\Delta t$ = 25 and 46 hours, respectively). In all cases, the nonreactive tracer tritium ($^3H_2O$) was injected simultaneously with the sorbing tracer to provide the basis for estimating physical transport parameters. The chemical composition of the tracer solutions is summarized in Table 2.

A consistent loss of tritium on the order of 10–13% was observed in all migration experiments. The explanation for this loss is uncertain; it may be related to the exchange with non-tritiated water within the experimental apparatus, fracture plane, or granite slabs, and/or to the conversion from decay counts (measured) to concentrations (calculated based on es-

**Table 1.** Experimental Conditions in Migration Experiments

| Experiment | Tracers | Injection | $\Delta t$, hours | $b$, $\mu$m | $V_f$, cm$^3$ | $Q$, cm$^3$ hr$^{-1}$ |
|---|---|---|---|---|---|---|
| 1 | $^{90}$Sr/$^3$H | pulse | 0.35 | 780 | 1.44 | 1.47 |
| 2 | $^{90}$Sr/$^3$H | finite step | 25 | 780 | 1.44 | 1.06 |
| 3 | $^{90}$Sr/$^3$H | finite step | 46 | 450 | 0.97 | 0.67 |

**Table 2.** Chemical Composition of Tracer Solutions

| Experiment | Tracer | Input $C_0$, Bq/mL | Background | $p$H |
|---|---|---|---|---|
| 1 | $^{90}Sr$ | 430 | $10^{-5}$ M $HNO_3$ | 5.5 |
| | $^{3}H$ | 916 | | |
| 2 | $^{90}Sr$ | 99.3 | $10^{-6}$ M $HNO_3$ | 5.7 |
| | $^{3}H$ | 617 | | |
| 3 | $^{90}Sr$ | 99.3 | $10^{-6}$ M $HNO_3$ | 5.7 |
| | $^{3}H$ | 617 | | |

timates of sample volume collected in fraction collector). The tritium breakthrough curves were adjusted to account for this loss. A similar loss of tritium was noted by *Hölttä et al.* [1991] in their migration experiments using an experimental design quite similar to the one used in our study.

After termination of the migration experiments the cores were dried and disassembled. Autoradiographs of the fracture surfaces were taken to examine the spatial distribution of the radioactive tracer remaining sorbed on the fracture surfaces.

### Static Sorption Experiments

Batch sorption measurements were carried out with strontium 90 and crushed Lac du Bonnet granite to determine the bulk sorption capacity of the granite matrix. The rock sample was wet-sieved through a 35–80 mesh (particle diameters ranging from 180 to 435 $\mu$m). Samples of one gram of dried rock were placed in polyethylene bottles and contacted with 10 mL of tracer solution containing strontium 90. Five initial tracer concentrations were used ranging from 50 to 2000 Bq/mL. All samples were shaken manually every 15 min and allowed to equilibrate for a total of 8 hours. Small aliquots of contacting solution were taken after 1, 4, and 8 hours and analyzed for strontium. Strontium sorption to the walls of the sample bottle was determined to be negligible.

Coupon sorption experiments were carried out to obtain independent estimates of the sorption capacity of the macrosurfaces of the polished granite. The experimental procedure is similar to that described by *Vandergraaf and Abry* [1982]. Small coupons were cut from core material, saturated with distilled water, and all sides but the one with the fracture surface were sealed with silicone rubber. The fracture surfaces were contacted with tracer solution by pipetting solution (2–3 $cm^3$) directly onto the surface (4–6 $cm^2$). A narrow rim of silicone rubber around the edges of the fracture surface contained the solution. In a sorption step, tracer solution with a chemical composition representative of that used in the migration experiments was added to the surface and allowed to equilibrate. The equilibration time for sorption ranged from 1 to 24 hours. In a subsequent desorption step the tracer solution was replaced by a tracer-free solution. For a given coupon the equilibration time for desorption was the same as previously allowed for sorption. The coupons were gently shaken throughout the experiment.

In a first set of experiments the contacting solutions were sampled only at the end of a specified equilibration time. The change in tracer concentration in the solution was used to calculate a surface distribution coefficient for the given equilibration time representing either sorption ($K_a^s$) or desorption ($K_a^d$). These $K_a$ values represent bulk estimates of solute partitioning which may include effects of matrix diffusion/sorption, especially in the cases with longer equilibration times. In a second set of coupon experiments, small aliquots of the contacting solution were taken as a function of time to measure the change in tracer concentration over time. A diffusion-sorption model is fit to these data to distinguish between (instantaneous) surface sorption and (time dependent) matrix diffusion/sorption. In all the coupon experiments, evaporation rates were measured to allow a correction of tracer concentration due to evaporation of solution.

### Interpretive Models

Assuming a zero initial concentration in the fracture and matrix, a constant concentration at the inlet of the fracture during tracer injection, and a matrix of large extension, the flux concentration $C_f(x, t)$ in the fracture is given [e.g., *Moreno et al.*, 1985] by

$$\frac{C_f}{C_0} = \frac{2}{\sqrt{\pi}} \exp\left(\frac{Pe}{2}\right) \int_p^\infty \exp\left(-\tau^2 - \frac{Pe^2}{16\tau^2}\right) \cdot \operatorname{erfc}\left(\frac{(Pe\, t_w G/8\tau^2)}{[t - (Pe\, t_0/4\tau^2)]^{1/2}}\right) d\tau \quad (5)$$

where

$$Pe = ux/D_L \quad (6)$$

$$p = \sqrt{Pe\, t_0/4t} \quad (7)$$

$$t_0 = R_a x/u = R_a t_w \quad (8)$$

$$G = a_w \sqrt{D_e K_a} \quad (9)$$

The parameter $G$ describes the influence of matrix diffusion/sorption on the concentration distribution in the fracture. For the range of fluid velocities used in our experiments, (5) is essentially equivalent to a solution based on an inlet boundary condition expressed as a "flux injection" [*Fujikawa and Fukui*, 1990]. A simpler model than (5) has recently been given by *Rasmussen* [1995].

The sorption experiments on granite coupons are interpreted using a diffusion-sorption model that describes the change in tracer concentration in the contacting solution due to surface sorption and matrix diffusion/sorption. In the coupon experiments the specific surface area $a_w$ is given as the inverse of the height $h$ of the water column contacting the coupon. Injection and detection are in the contacting solution and the delta-type fluid injection takes the form [*Fujikawa and Fukui*, 1990]

$$C_0 = \frac{M\delta(t)}{V\left(1 + \frac{1}{h} K_a\right)} \quad (10)$$

where $V$ is the volume of the contacting solution and $M$ is the total mass (or activity) of tracer added. Note that the surface distribution coefficient $K_a$ appears in the initial condition (10). Under the assumption of instantaneous sorption the solute sorbs to the surface at the moment of tracer injection and therefore, from the beginning, the solute exists in both the solution phase and on the surface of the coupon. The principle of mass conservation requires that the initial tracer concentration in the contacting solution be reduced by the magnitude of the term $(1 + K_a/h)$ (see *Fujikawa and Fukui* [1990] for details).

Assuming zero initial concentration throughout the rock

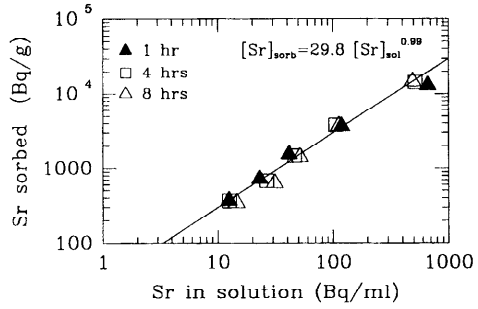


**Figure 2.** Experimental results of batch sorption of strontium on crushed granite particles (180–435 $\mu$m) for 1, 4, and 8 hours equilibration time. A least squares fit to all data (solid line) suggests a linear Freundlich isotherm ($R^2 = 0.98$).

matrix and diffusion distances much shorter than the thickness of the granite coupons (i.e., $\ll$2 cm), the change in tracer concentration in the contacting solution is given by [*Neretnieks*, 1980]:

$$C_r/C_0 = \exp(\theta)\ \mathrm{erfc}(\sqrt{\theta}) \tag{11}$$

where the dimensionless time $\theta$ is

$$\theta = \frac{D_e K_v}{h^2} t \tag{12}$$

The diffusion-sorption model is used to determine $K_a$ values describing instantaneous surface sorption as follows. First, the solution (11) is fit to the observed concentration-time trends using a fixed value of the $D_eK_v$ parameter estimated from batch sorption measurements of $K_D$ and literature values of $D_e$, $\rho_s$, and $\varepsilon_p$. In this way, the initial concentration $C_0$ defined in (10) is the only fitting parameter. Second, the surface distribution coefficient $K_a$ is calculated from the best fit $C_0$ and the known mass $M$ of tracer initially introduced according to

$$K_a = h\left(\frac{M}{VC_0} - 1\right) \tag{13}$$

The calculated $K_a$ values express the loss of tracer from solution due to instantaneous sorption only.

## Results and Discussion

### Static Sorption Experiments

Batch sorption measurements of stronium 90 on crushed granite suggest a linear Freundlich isotherm for the concentration range of interest (Figure 2). The influence of equilibration time (1–8 hours) on the distribution of tracer between rock surfaces and solution is negligible. The least squares fit of the Freundlich isotherm gives a bulk distribution coefficient of $K_D$ = 29.5 mL/g. The linearity of the strontium sorption isotherm has been demonstrated in other batch sorption experiments [e.g., *Skagius et al.*, 1982]. The bulk distribution coefficient determined here is somewhat higher than what has been observed in similar batch sorption experiments. *Torstenfelt et al.* [1982] reported $K_D$ values ranging from 5 to 20 mL/g for strontium on granite samples from Sweden. *Vandergraaf et al.* [1994] obtained a $K_D$ value of 1.3 ± 0.1 mL/g for strontium on granites similar to those used in our experiments. The low ionic strength of the background solution used in this study (Table 2) is likely responsible for the relatively high bulk distribution coefficient. A lower ionic strength of the background solution provides fewer cations to compete with strontium for the existing sorption sites. As a result, a greater amount of strontium sorbs to the solid phase and the value of $K_D$ increases. When interpreting the coupon and migration experiments, we will assume that the value of $K_D$ estimated from batch tests using crushed granite is representative of the sorption properties of intact granite.

Surface distribution coefficients for strontium, estimated from the coupon experiments, are summarized in Table 3. Recall that a "bulk estimate" of $K_a$ is based on the total partitioning of the solute between the solid phase and solution (including possible sorption within the matrix). To examine the influence of equilibration time on sorption, three granite coupons were exposed to tracer solution and the change in tracer concentration was monitored over time (Figure 3). The mass (activity) of strontium initially introduced to the solution is shown for comparison (labeled as concentration $M/V$, Figure 3). Figure 3 shows that most of the sorption took place during the first hour (or possibly minutes) of contact, after which time sorption increased at a fairly slow rate. The sorption time trends are very similar for all three coupons. *Torstenfelt et al.* [1982] observed similar time trends of strontium sorption on granite macrosurfaces. They suggested that the first rapid phase corresponds to sorption on externally accessible surfaces, while the second phase might reflect diffusion-controlled mass transport into microfissures and internal exchange sites.

To separate the effects of fast surface sorption and slow matrix diffusion/sorption, the observed concentration-versus-time trends are modeled using a diffusion-sorption model (equation (11)). For simplicity, we use an independent estimate of $D_eK_v$ and fit the model by varying only $C_0$. Assuming an effective diffusivity for strontium of $1 \times 10^{-12}$ m$^2$/s [*Skagius et al.*, 1982] and using a value of $K_v$ = 78.2 based on $K_D$ = 29.5 mL/g determined from the batch sorption isotherm (Figure 2), the best fits of the diffusion-sorption model are shown

**Table 3.** Summary of Surface Distribution Coefficients Determined in Coupon Sorption Experiments of Strontium on Polished Granite

| Type of Estimate | Contact Time, hour | Number of Samples | $K_a^s$, cm | $K_a^d$, cm |
|---|---|---|---|---|
| Bulk[a] | 1–2 | $n$ = 4 | 0.07 ± 0.03 | 0.11 ± 0.03 |
| Bulk[a] | 6 | $n$ = 3 | 0.19 ± 0.02 | 0.32 ± 0.01 |
| Model[b] | "instantaneous" | $n$ = 3 | 0.09–0.13 | 0.16–0.48 |

[a]Average and standard deviation from "bulk measurements"; no correction made for matrix diffusion/sorption.

[b]Range of $K_a$ values for three coupons describing instantaneous sorption (Figure 2) and instantaneous desorption (Figure 3) (see text).

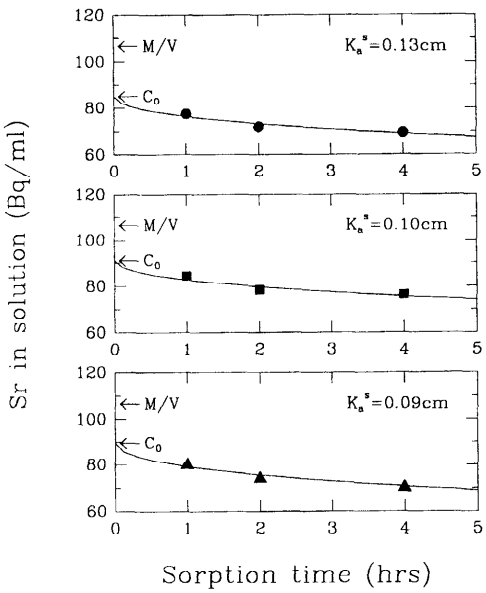


**Figure 3.** Sorption of strontium to three granite coupons as a function of time. The best fit of the diffusion/sorption model (solid line) assuming $D_e K_v = 7.8 \times 10^{-11}$ m$^2$/s was used to determine $C_0$ and $K_a^s$ (see text).

in Figure 3 as solid lines. The best fit value of $C_0$ is indicated for reference. The diffusion-sorption model describes the experimental data well, suggesting that matrix diffusion/sorption could explain the slow decline in tracer concentration over time. The estimate of $K_a$ is calculated from the best fit value of $C_0$ and the known mass $M$ of tracer initially introduced (see equation (13)). For the three granite coupons shown in Figure 3 we obtain estimates of $K_a^s$ (describing instantaneous surface sorption) ranging from 0.09 to 0.13 cm (Table 3). It appears inconsistent that these model estimates of $K_a^s$ for "instantaneous sorption" are slightly higher than bulk estimates of $K_a^s$ for 1–2 hours sorption time (Table 3). However, one should keep in mind that the bulk and model estimates were determined on different granite coupons. Natural variability in sorption properties of different coupons (and perhaps small differences in the experimental setup) could have caused this apparent inconsistency in the sorption trends with time. For a given coupon, however, the model estimates of instantaneous sorption were always smaller than bulk estimates calculated after a few hours.

The desorption trends as a function of time for the three granite coupons are shown in Figure 4. An initial, fast desorption was followed by a relatively slow rate of further release of tracer into the solution. Unfortunately, the diffusion-sorption model cannot be applied here due to uncertainty in the initial and boundary conditions. As a first approximation, a straight line is fit to the experimental data to obtain an approximate estimate of the amount of strontium desorbed instantaneously. This estimate is then used to calculate surface distribution coefficients $K_a^d$ representing instantaneous desorption for any given coupon. According to model calculations a significant fraction of the tracer (~60%) moved into the matrix during the sorption step. Assuming that this tracer fraction did not participate in the initial desorption, the estimates of $K_a^d$ range from 0.16 to 0.48 cm (Table 3).

A comparison of the various estimates of $K_a^s$ and $K_a^d$ (Table 3) shows that the $K_a^s$ values are systematically lower than $K_a^d$ values, suggesting hysteresis in the sorption process. In the case of bulk estimates, some of the discrepancy between $K_a^s$ and $K_a^d$ is caused by matrix diffusion/sorption which releases a sorbed tracer only slowly from the matrix. However, the effects of matrix diffusion/sorption are removed in the estimates of $K_a^s$ and $K_a^d$ based on the diffusion/sorption model. The fact that this latter estimate of $K_a^d$ is significantly greater than the estimate of $K_a^s$ strongly suggests that strontium exhibited hysteresis in the sorption process under the experimental conditions used here.

Hysteresis between adsorption and desorption is commonly observed, with desorption taking more time than adsorption to attain equilibrium [*Davis and Kent*, 1990]. Batch experiments by *Barney* [1984] demonstrated that the magnitude of this hysteresis depends not only on the solute chemistry but also on the experimental conditions (e.g., temperature, redox conditions, and ionic strength). The low ionic strength of the background solution (Table 2) probably favored slow desorption and/or partially irreversible sorption as few ions could compete with strontium for the sorption sites. *Vandergraaf and Abry* [1982] observed an even higher degree of hysteresis for strontium 90 sorption/desorption on granite during coupon sorption experiments using synthetic groundwater and longer equilibration times (14–28 days). In their experiments surface distribution coefficients for sorption ($K_a^s$ = 0.09–0.17 cm) and desorption ($K_a^d$ = 1.8–2.6 cm) differed by one order of magnitude. Unfortunately, the reported values of $K_a$ are bulk estimates only. It is not clear how much of this discrepancy is due to an apparent hysteresis caused by matrix diffusion/sorption.

### Analysis of Tritium Breakthrough Curves

The breakthrough curves (BTCs) of the nonsorbing tracer tritium are used to determine the hydraulic parameters ($Pe$, $t_w$). The relatively short water residence time ($t_w \sim 1$ hour) did not allow a determination of the diffusion parameter G (equation (9)). For a nonsorbing solute, $G$ takes the form $G = a_w(D_e\varepsilon_p)^{1/2}$. Given the range of values one can expect for the

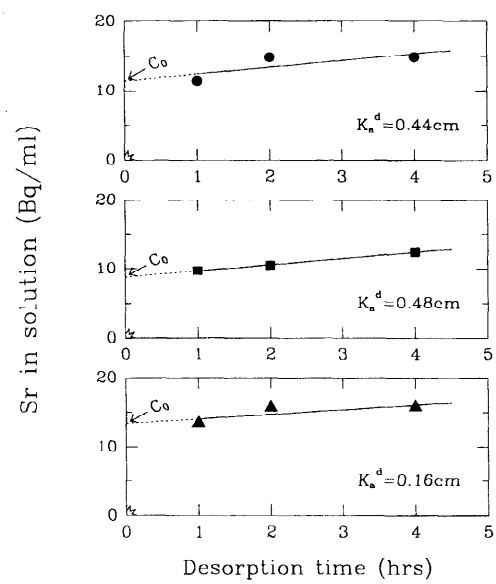


**Figure 4.** Desorption of strontium from three granite coupons as a function of time. A straight line was fit to the data to estimate $C_0$.

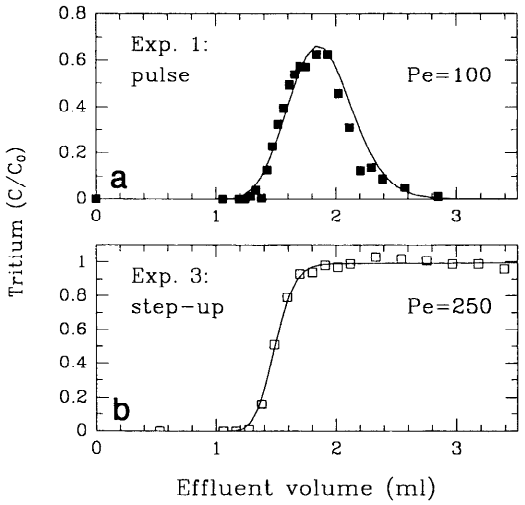


**Figure 5.** Experimental breakthrough of tritium in response to (a) a pulse injection (experiment 1) and (b) a finite step injection (experiment 3). The lines represent the best (visual) fit of the transport model (1)–(4).

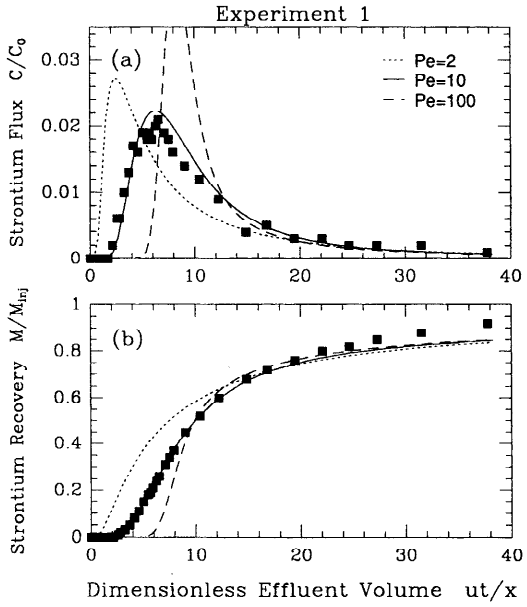


**Figure 6.** Experimental breakthrough of strontium (squares) and model simulations for experiment 1 assuming $D_e K_v = 7.8 \times 10^{-11}$ m$^2$/s and (1) $Pe = 2$ (dotted line), (2) $Pe = 10$ (solid line), (3) $Pe = 100$ (dashed line). (a) Normalized effluent concentration; (b) normalized mass recovery.

effective diffusivity of tritium in granite ($D_e = 0.7$–$1.8 \times 10^{-13}$ m$^2$/s [*Moreno et al.*, 1985]) and porosity in Lac du Bonnet granites ($\varepsilon_p = 0.02$–$0.04$), the influence of $G$ on the breakthrough curve is negligible. We assumed $D_e = 1.0 \times 10^{-13}$ m$^2$/s and $\varepsilon_p = 0.03$ in order to determine the remaining parameters ($Pe$, $t_w$).

Figure 5 shows the experimental BTCs of tritium for experiments 1 and 3. The near-symmetrical shape of the BTCs suggests that a Fickian-type dispersion model is applicable. The analytical solution fits the data fairly well. Significant outliers are believed to be a result of experimental error such as variability in drop size during sampling. The hydraulic parameters $Pe$ and $t_w$ are summarized in Table 4. From these values the dispersion coefficient and the total volume $V_t$ are calculated. The total volume $V_t$ includes additional volumes above the fracture volume due to tubing and inflow/outflow plenums and is calculated from the measured flow rate and the residence time $t_w$. The values of $V_t$ agree to within 10% with independent estimates of $V_t$ based on the calculated volumes of fracture and tubing.

The relatively high Peclet numbers ($\geq$100) indicate that advective transport dominated over dispersive transport in all experiments (Table 4). Dispersive effects are largely determined by the combined influence of mixing in the instrumentation, diffusive mixing across the width of the fracture, and the development of an enhanced velocity profile across the width of the fracture. Dye experiments in acrylic replicates of the fractures suggest this velocity profile is due to an entrance effect introduced by the inflow reservoir. While influencing the magnitude of $D_L$, this inlet effect does not compromise our evaluation of the sorption process.

The experimental setup used for the pulse injection results in more dispersion than the setup used for the continuous injection (Table 4). It is likely that some mixing occurred between the injected tracer slug and the background solution before the tracer slug entered the fracture. This "smearing" of the tracer slug could explain the greater dispersion in the tritium elution profile in experiment 1. The estimated dispersion coefficients are essentially the same for the large-aperture and smaller-aperture fractures (experiments 2 and 3), suggesting that Taylor dispersion across the aperture is a minor component of the total dispersion.

**Table 4.** Summary of Hydraulic Parameters Determined for Migration Experiments in Fractures of Granite Using the Transport Model (1)–(4) Based on Tritium

| Experiment | Fluid[a] Residence Time $t_w$, hour | Total Volume $V_t$, cm$^3$ | Peclet Number[a] | Dispersion Coefficient[b] $D_L$, cm$^2$ hr$^{-1}$ |
|---|---|---|---|---|
| 1 | 1.3 | 1.62 | 100 | 0.76 |
| 2 | 1.4 | 1.47 | 250 | 0.29 |
| 3 | 1.6 | 1.07 | 250 | 0.25 |

[a]Based on visual fit; uncertainty estimated to be ±10%.
[b]Calculated assuming $x = 10$ cm.

### Influence of Nonideal Sorption on Dispersion of Strontium

In migration experiment 1 we focus on the influence of nonideal sorption on the transport of strontium. Figure 6 shows the observed breakthrough of strontium (squares) in response to a short pulse injection. Figure 6a shows the instantaneous breakthrough curve as a function of dimensionless effluent volume. A dimensionless effluent volume of one corresponds to one total fracture volume $V_t$. The mass recovery is shown in Figure 6b. The mass recovery curve illustrates how much of the injected tracer mass is lost from the fracture because of matrix diffusion/sorption and/or irreversible sorption [e.g., *Maloszewski and Zuber*, 1990]. The breakthrough curve shows a steep rise with an early peak and significant tailing (Figure 6a). This asymmetry was not observed for tritium (Figure 5a). Clearly, strontium exhibits more dispersion than the nonreactive tracer. Note that this "enhanced disper-

sion" results in lower retardation of the peak ($R_{peak}$ = 6.4) relative to retardation of the center of mass ($R_{COM}$ = 10.0). Using the definition of the surface retardation factor (2), we obtain surface distribution coefficients ranging from $K_a$ = 0.21 cm (based on peak retardation) to $K_a$ = 0.35 cm (based on center of mass retardation). These estimates of the sorption strength fall within the range of $K_a$ values determined in coupon sorption experiments (Table 3).

The degree to which dispersion is enhanced because of sorption is modeled implicitly by increasing the value of the dispersion coefficient in (1) beyond the value of $D_L$ determined for tritium. In using this effective dispersion coefficient ($D_{eff}$) we assume that enhanced dispersion due to sorption is Fickian. We compare three scenarios with (1) hydrodynamic dispersion only ($D_{eff} = D_L$ = 0.76 cm$^2$/s; $Pe$ = 100), (2) enhanced dispersion ($D_{eff}$ = 7.6 cm$^2$/s; $Pe$ = 10), and (3) strongly enhanced dispersion ($D_{eff}$ = 38 cm$^2$/s; $Pe$ = 2). We adopt the same diffusion/sorption capacity $D_eK_v = 7.8 \times 10^{-11}$ m$^2$/s used earlier for modeling the coupon experiments. The sorption potential to the fracture surface ($K_a$) is held constant in all three simulations. We use the average value of the model estimates (Table 3) for $K_a^s$ (instantaneous sorption) and $K_a^d$ (instantaneous desorption); that is, $K_a$ = 0.25 cm. We emphasize that the model is used here for comparative purposes rather than for fitting of transport parameters.

The results of these three scenarios are shown in Figure 6. A calculation assuming a Peclet number of 100 produces a narrower, more symmetric peak, and significantly higher peak concentrations than are observed (Figure 6a). Only the tail of the breakthrough curve is reproduced by this model, suggesting that the process of matrix diffusion/sorption may explain the significant tailing. However, it can not explain the observed broadening of the peak and the reduction in peak height. Clearly, additional dispersion has occurred as a result of chemical interaction with the fracture surfaces. The good fit of the transport model to the strontium data for $Pe$ = 10 suggests that the dispersion of strontium is approximately an order of magnitude greater than that experienced by the nonreactive tracer tritium.

An inspection of the recovery curves (Figure 6b) shows that the final mass recovery is virtually independent of the degree of dispersion in the fracture. Instead, diffusion into and sorption within the rock matrix controls the tailing behavior and the final mass recovery. Using our independent estimate of the matrix diffusion/sorption parameter ($D_eK_v = 7.8 \times 10^{-11}$ m$^2$/s) the transport model predicts a tracer mass recovery of ~85% after 40 dimensionless effluent volumes. These predictions agree fairly well with the observed strontium recovery of ~92%, suggesting that our estimate of $D_eK_v$ (based on $K_D$ from the batch isotherm) is a good first approximation for the diffusion/sorption parameter.

The following three processes may have contributed to the additional dispersion observed for strontium: (1) chemical heterogeneity, (2) hysteresis in sorption, and (3) limited transverse mixing across the fracture aperture. The influence of chemical heterogeneity on dispersion of sorbing solutes is well documented for the case of a porous medium [e.g., *Brusseau and Rao*, 1989; *Tompson*, 1993]. The same principles would apply to a fracture, namely an increase in dispersion with an increase in spatial variability in sorption sites and/or sorption strength. Autoradiographs of the fracture surfaces, taken after completion of experiment 1, revealed a very heterogeneous ("spotty") spatial distribution of the strontium remaining sorbed on the surface. This chemical heterogeneity is at the scale of the mineral grains (1–2 mm). Similar spatial distributions of sorbed activity were found in experiments 2 and 3. These observations are consistent with results from several studies which have demonstrated that the various minerals making up a granite vary in their general sorptive capacity as well as their specific affinity for sorption of strontium [e.g., *Torstenfelt et al.*, 1982; *Ticknor et al.*, 1986]. Hence chemical heterogeneity could have contributed to the enhanced dispersion of strontium.

Hysteresis of sorption may also cause enhanced dispersion due to differences in retardation of the front and tail of the tracer pulse. Retardation of the front of the tracer pulse is effectively controlled by sorption to the fracture walls, whereas the retardation of the tail of the tracer pulse is controlled by desorption from the fracture walls. It follows that the tail of the pulse is retarded more (higher $K_a^d$) than the front of the pulse (lower $K_a^s$) causing an increase in plume spreading. The significant hysteresis of strontium observed during static sorption to granite macrosurfaces ($K_a^d > K_a^s$, Table 3) likely contributed to the enhanced dispersion of strontium in the migration experiment.

A third process, limited transverse mixing, may also be contributing to enhanced dispersion. Model calculations by C. Wels et al. (The influence of surface sorption on dispersion in parallel-plate fractures, submitted to *Journal of Contaminant Hydrology*, 1996, hereinafter referred to as C. Wels et al., submitted manuscript, 1996) suggest that under the assumption that solute must move into close vicinity of the fracture wall to participate in the sorption process, the longitudinal transport distance required to establish transverse homogenization is proportionally longer by the magnitude of the surface retardation factor, and the negative correlation between the probability of sorption and the magnitude of the local velocity along the parabolic velocity profile creates additional dispersion. The degree to which a solute participates in surface sorption depends upon the degree of transverse mixing across the aperture, which can be characterized in terms of a transverse Peclet number $Pe_t = ub/D_m$. For $Pe_t < 2$ the diffusion distance is sufficiently small to approximate "instantaneous transverse mixing." For $Pe_t > 2$ the rate of transverse mixing relative to the advective transport is limited, creating the situation where the correlation between the probability of sorption and the local advective velocity leads to enhanced dispersion. In experiment 1 the transverse Peclet number was $Pe_t$ = 14.8, suggesting that transverse mixing was indeed limited. In accord with model calculations by C. Wels et al. (submitted manuscript, 1996), the transport and sorption conditions in experiment 1 ($Pe_t$ = 14.8; $R_a$ ~ 7.5) would result in an approximate tenfold increase in Taylor dispersion for the sorbing tracer strontium ($Pe_{L;\,sorbing}$ ~ 100) relative to that of a conservative solute ($Pe_L = 210D_mL/[u\langle b^2\rangle]$ ~ 1000). Similarly, the critical entrance length required to establish transverse homogenization would increase from ~0.5 cm for a conservative solute to ~3.75 cm for the sorbing solute strontium.

In summary, the sorbing solute strontium exhibited approximately an order of magnitude more dispersion than predicted from the breakthrough of the nonreactive tracer tritium. We can only speculate on the relative importance of chemical heterogeneity, hysteresis, and limited transverse mixing in contributing to enhanced dispersion of strontium during experiment 1. The coupon sorption experiments suggest that chem-

ical heterogeneity and hysteresis are interrelated. The range of instantaneous $K_a$ values determined for three different coupons (i.e., chemical heterogeneity) was much greater during the desorption step (Figure 4) than during the sorption step (Figure 3). More in-depth studies on these complex, nonideal sorption processes are needed in order to quantify their respective influence on solute dispersion in fractures.

### Influence of Fracture Aperture on Retardation of Strontium

The influence of fracture aperture on strontium transport is best illustrated by direct comparison of the breakthrough curves in experiments 2 and 3 (Figure 7). In experiment 2, two short, but significant, deviations from the general trend occurred as a result of sudden changes in strontium concentrations in the inflow reservoir. The spike of $C/C_0$ observed at about six effluent volumes was in response to an (accidental) increase of 10% in the strontium concentration in the inflow reservoir. The short but significant drop in $C/C_0$ at about 18 effluent volumes was in response to switching from strontium containing input solution to tracer-free background solution (end of step injection). These short-term effects are not considered further in our analysis.

Two general observations can be made regarding the influence of fracture aperture on strontium transport. First, the retardation of strontium is significantly greater in the smaller-aperture fracture than in the large-aperture fracture. For example, the first significant breakthrough of strontium (e.g., $C/C_0 > 0.025$) is observed after 1.5 fracture volumes in the large-aperture fracture. In the smaller-aperture fracture, however, approximately 8.7 fracture volumes were required to elute the same breakthrough fraction. Second, the strontium breakthrough is more dispersed and tracer concentrations are lower in the fracture with the smaller aperture compared to that with a large aperture. For example, the peak effluent concentration in the large-aperture fracture is approximately $C_{peak}/C_0 = 0.55$ compared to only $C_{peak}/C_0 = 0.30$ in the smaller-aperture fracture.

These observations agree qualitatively with the theoretical predictions from the transport model (1)–(4). According to this model a larger specific surface area (i.e., a smaller aperture) results in (1) increased retardation and (2) increased loss of tracer from the fracture to the matrix and tailing in the effluent. In the following, we compare the experimental data to simulated breakthrough curves using the transport model (1)–(4). The purpose of this comparison is to test whether the differences in strontium breakthrough in experiments 2 and 3 can be explained by the difference in fracture aperture. In theory, a single set of parameter values for $Pe$, $K_a$, and $D_eK_v$ should describe both experimental breakthrough curves.

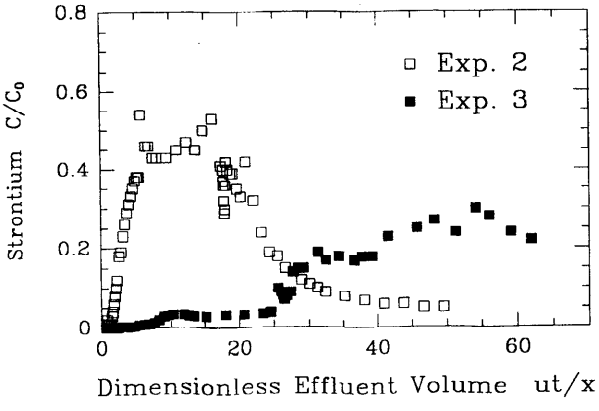


**Figure 7.** Comparison of experimental breakthrough of strontium in experiment 2 ($b$ = 780 $\mu$m; open squares) and experiment 3 ($b$ = 450 $\mu$m; solid squares).

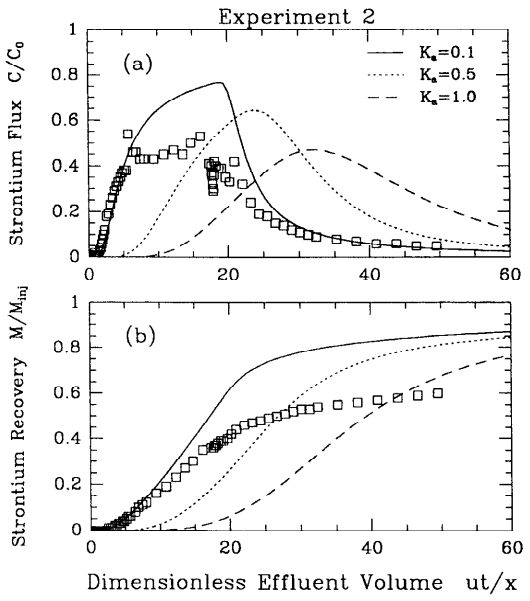


**Figure 8.** Experimental breakthrough of strontium (squares) and model type curves for experiment 2 ($b$ = 780 $\mu$m) assuming (1) $K_a$ = 0.1 cm (solid line), (2) $K_a$ = 0.5 cm (dotted line), (3) $K_a$ = 1.0 cm (dashed line). The diffusion/sorption parameter is $D_eK_v = 7.8 \times 10^{-11}$ m$^2$/s in all three simulations.

An extensive comparison of transport simulations with the experimental data for a wide range of $Pe$, $K_a$, and $D_eK_v$ values yielded two general conclusions. First, the transport model fitted the breakthrough curves in both experiments very poorly when $Pe$ = 250, which is the estimate of $Pe$ from the tritium BTC (Table 4). The Peclet number had to be decreased by an order of magnitude to account for enhanced dispersion. Second, no single parameter set ($Pe$, $K_a$, and $D_eK_v$) could be found that would describe the experimental data in both experiments equally well. In particular, $K_a$ had to be varied greatly to obtain acceptable fits. To illustrate this point, we show three model "type curves" for experiments 2 and 3, assuming (1) $K_a$ = 0.1 cm, (2) $K_a$ = 0.5 cm, and (3) $K_a$ = 1.0 cm. For simplicity, we set $Pe$ = 10, which assumes that the magnitude of enhanced dispersion in experiments 2 and 3 is equal to that estimated for experiment 1. In these calculations we also assume $D_eK_v = 7.8 \times 10^{-11}$ m$^2$/s as used earlier for modeling the sorption time trends (Figure 3).

Figures 8 and 9 show the simulated type curves (lines) for experiments 2 and 3, together with the experimental data (symbols). Instantaneous breakthrough curves are shown in Figures 8a and 9a and mass recovery curves are shown in Figures 8b and 9b. In experiment 2 the type curve with $K_a$ = 0.1 cm describes the retardation in the arrival time of the peak of the plume fairly well (Figure 8a). This value of $K_a$ is within the range of estimates of $K_a$ determined from coupon sorption experiments (Table 3). In contrast, the same type curve signif-

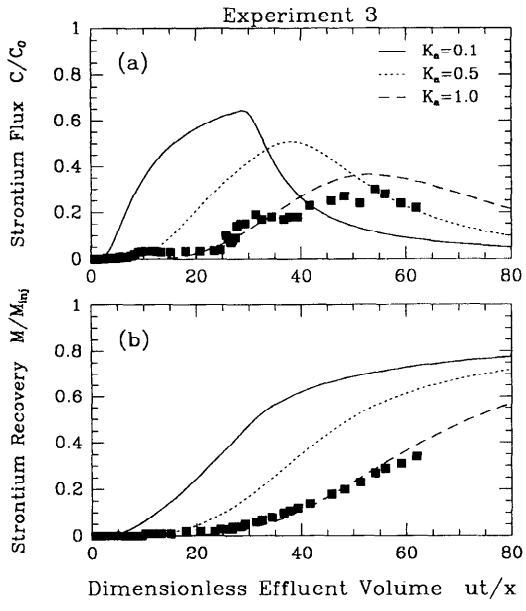


**Figure 9.** Experimental breakthrough of strontium (squares) and independent model predictions for experiment 3 ($b$ = 450 $\mu$m) assuming (1) $K_a$ = 0.1 cm (solid line), (2) $K_a$ = 0.5 cm (dotted line), (3) $K_a$ = 1.0 cm (dashed line). The diffusion/sorption parameter is $D_eK_v = 7.8 \times 10^{-11}$ m$^2$/s in all three simulations.

icantly underestimates the retardation of strontium observed in experiment 3 (Figure 9a). The $K_a$ value has to be increased by one order of magnitude ($K_a$ = 1.0 cm) to model the observed retardation in this experiment. These model results indicate that strontium sorbed much more extensively to the fracture walls during experiment 3 than during experiment 2. Additional results not shown here indicated that strontium retardation is considerably more sensitive to $K_a$ than to $D_eK_v$, suggesting that differences in surface sorption rather than in matrix diffusion/sorption caused the large differences in retardation between the two experiments. Note that the difference between the $K_a$ values required to match the strontium breakthrough curves is significantly greater than the variability in the $K_a$ values determined in coupon sorption experiments (Table 3). Hence we do not believe that natural variability in sorption between the fracture surfaces caused the different retardation response in experiments 2 and 3.

In our opinion, the difference in the extent of sorption of strontium is caused by the difference in specific surface area of the fracture in experiment 2 ($b$ = 780 $\mu$m) and experiment 3 ($b$ = 450 $\mu$m). This contention is supported by the fact that the simulation results for experiment 2 are consistent with those for experiment 1 which was also conducted in a large-aperture fracture ($b$ = 780 $\mu$m). In both experiments the estimates of sorption strength agree fairly well ($K_a$ = 0.25 cm in experiment 1 versus $K_a$ = 0.1 cm in experiment 2), despite the differences in tracer injection. We emphasize that our results suggest that the distribution of tracer between surface and aqueous phase (i.e., $K_a$) is a function of the specific surface area $a_w$ of the fracture. This is not to be confused with the commonly assumed influence of $a_w$ on the retardation factor $R_a$ (= 1 + $a_wK_a$) which follows from the partitioning of tracer mass between surface and solution. A positive correlation of $K_a$ with $a_w$ results in a much stronger (nonlinear) influence of specific surface area on retardation (as observed in our experiments) than is commonly assumed in the retardation model (equation (2)).

Two factors may have contributed to the observed increase in the extent of sorption with an increase in specific surface area $a_w$ of the fracture. The first factor relates to the limited access of the tracer to the sorbing surface during advection-dominated transport (see previous section). Recall that a transverse Peclet number greater than 2 indicates that mixing across the aperture is limited due to the high advective flow rate relative to the rate of transverse diffusion. The transverse Peclet numbers for experiment 2 ($b$ = 780 $\mu$m) and experiment 3 ($b$ = 450 $\mu$m) were $Pe_t$ = 10.0 and $Pe_t$ = 5.7, respectively. In other words, transverse mixing and access to the fracture walls was limited to a greater extent in the large-aperture fracture (greater diffusion distance) relative to the smaller-aperture fracture.

The second factor relates to the nonideal sorption behaviour of strontium. A comparison of the mass recovery of strontium in the three migration experiments suggests that hysteresis (i.e., slow desorption rates) has a much stronger influence on strontium transport in the case of a finite step injection on the order of 1–2 days (experiments 2 and 3) compared to a short pulse injection on the order of less than 1 hour (experiment 1). For example, in the large-aperture fractures, 92% of the injected strontium was recovered in experiment 1 ($\Delta t$ = 0.35 hour; Figure 6b) compared to 60% in experiment 2 ($\Delta t$ = 25 hour; Figure 8b) and only 35% in experiment 3 ($\Delta t$ = 46 hour; Figure 9b).

The low tracer recovery is probably a result of the low extent of desorption. The "average retardation" of the solute plume in experiment 1 could be modeled using the average of the instantaneous estimates (Table 3) for sorption and desorption (i.e., $K_a = (K_a^s + K_a^d)/2$ = 0.25 cm). The modeling of the strontium retardation in experiment 3, however, indicated a much higher "average" distribution coefficient ($K_a$ = 1.0 cm). Assuming a decrease in the extent of desorption is responsible, we obtain an approximate distribution coefficient for desorption of $K_a^d$ = 1.9 cm (= $2K_a - K_a^s$). In experiment 2, such an estimation of $K_a^d$ from the "average retardation" of strontium is not meaningful since a large fraction of strontium sorbed irreversibly. It is clear, however, that the extent of desorption was much lower (i.e., higher $K_a^d$) than estimated for experiment 1.

We speculate that the different magnitude of hysteresis is a result of the difference in sorption time. A longer duration of tracer injection results in a longer residence time of the tracer sorbed onto the surface. Results of coupon sorption experiments not shown here suggested that an increase in equilibration time during a sorption step decreased the extent of desorption during a subsequent desorption step. Longer sorption times may allow an incorporation of the tracer into the mineral lattice. These new chemical bonds can be expected to have greater activation energies for dissociation [e.g., *Davis and Kent*, 1990]. The possible influence of sorption time on hysteresis and its effects on transport of the sorbing solute is a subject worth further study.

In conclusion, retardation of strontium was approximately 13 times greater during transport in a smaller-aperture fracture ($b$ = 450 $\mu$m) compared to that in a large-aperture fracture ($b$ = 780 $\mu$m). This increase in retardation is much greater than predicted by the commonly used definition of the surface retardation factor (equation (2)). A combination of hysteresis

of sorption and limited transverse mixing could explain the observed strong influence of fracture aperture on the retardation and mass recovery of strontium.

## Implications for Reactive Transport in Fractured Media

A number of authors have adopted the concept of retardation in their analysis of transport of sorbing solutes in fractured media [e.g., *Neretnieks et al.*, 1982; *Moreno et al.*, 1985; *Dverstorp et al.*, 1992; *Fujikawa et al.*, 1993; *Moreno and Neretnieks*, 1993; *Wels and Smith*, 1994]. The retardation model assumes that retardation of the solute in the fracture varies in proportion to the extent of sorption ($K_a$) and the specific surface area ($a_w = 2/b$) (see equation (2)). This model implies that retardation increases with a decrease in fracture aperture whereas the extent of sorption of a solute is independent of fracture aperture (or $a_w$). The assumed linear dependence of retardation on fracture aperture has important implications for transport in fractured media. Numerical studies have shown that this dependence would result in nonuniform and anisotropic retardation at the network scale [*Wels and Smith*, 1994]. By analogy, the same concept may apply to reactive transport in rough-walled fractures where retardation in a given channel is inversely proportional to channel aperture [*Neretnieks et al.*, 1982].

Our experimental results suggest that the influence of fracture aperture on the extent of retardation may be greater than assumed by the retardation equation (2) for those sorbing solutes that exhibit hysteresis in surface sorption. Our findings suggest that the extent of sorption ($K_a$) may increase with decreasing fracture aperture (increasing $a_w$) thus magnifying the influence of specific surface area on retardation. The observed dependence of $K_a$ on fracture aperture would significantly increase the complexity of solute transport either in rough-walled fractures or in networks of fractures. In particular, we anticipate a greater degree of nonuniformity and anisotropy in retardation at the plume scale.

We have suggested that hysteresis in sorption caused the significant increase in strontium retardation in the smaller-aperture fracture. However, other nonideal effects in sorption such as nonlinear and/or nonequilibrium sorption may also cause a nonlinear dependency of retardation on fracture aperture. Given its potential to significantly influence retardation at the plume scale, the relationship between retardation and fracture aperture should be examined for a range of solutes and transport conditions. It should be noted that migration experiments in natural, rough-walled fractures may not be ideal for this purpose because of the difficulties in characterizing the aperture distribution and the resulting dispersion and/or channeling. In our opinion, migration experiments in fractures of simple geometry are best suited for studying the influence of fracture aperture on retardation.

## Conclusions

Laboratory migration experiments using the sorbing radionuclide strontium 90 in constant-aperture fractures were carried out to study the influence of the specific surface area of a fracture on reactive solute transport. The following conclusions are drawn from the experimental observations:

1. Strontium exhibited nonideal sorption behavior on granite surfaces. Static sorption experiments on coupons suggested a hysteresis in the sorption process, showing higher surface distribution coefficients for desorption than for sorption (i.e., $K_a^d > K_a^s$). Estimates of instantaneous surface sorption ranged from $K_a^s = 0.09$–$0.13$ cm for sorption to $K_a^d = 0.16$–$0.48$ cm for desorption.

2. Strontium experienced significantly more dispersion than the nonreactive tracer tritium. This enhanced dispersion is believed to be a result of chemical heterogeneity, hysteresis in sorption, and limited transverse mixing across the fracture aperture. For the pulse injection the retardation of the peak ($R_{peak} = 6.4$) and the center of mass ($R_{50} = 10.0$) of the strontium breakthrough curve is consistent with model simulations using an independent estimate of the surface distribution coefficient from static sorption experiments ($K_a = 0.25$ cm).

3. The influence of fracture aperture on retardation is significantly greater than predicted by the commonly used definition of the surface retardation factor (equation (2)). Strontium retardation was approximately an order of magnitude greater in a smaller-aperture fracture (450 $\mu$m, $R_a \sim 45$) than in a large-aperture fracture (780 $\mu$m, $R_a \sim 3.5$) using step injections of 1 and 2 days, respectively. We hypothesize that hysteresis in sorption, in conjunction with limited transverse mixing across the aperture, caused the apparent increase in sorption strength ($K_a$) with a decrease in fracture aperture.

4. The results suggest that the magnitude of hysteresis increases with the residence time of the sorbing solute in the fracture. For example, in the large-aperture fracture, 92% of the injected strontium was recovered in response to a short pulse injection ($\Delta t = 0.35$ hour) compared to only 60% in response to a finite step injection ($\Delta t = 24$ hour).

## Notation

$a_w$ specific surface area of fracture, cm$^2$/cm$^3$.
$b$ fracture aperture, $\mu$m.
$C_f$ concentration in the mobile fluid in the fracture, Bq/mL.
$C_p$ concentration in the stagnant fluid in the matrix, Bq/mL.
$C_r$ concentration in solution contacting rock coupons, Bq/mL.
$C_0$ initial concentration, Bq/mL.
$D_m$ molecular diffusion coefficient in water, cm$^2$/hr.
$D_e$ effective diffusivity of rock matrix, $\varepsilon_p \tau D_m$, cm$^2$/hr.
$D_L$ longitudinal dispersion coefficient, cm$^2$/hr.
$h$ height of water column in static sorption experiments, cm.
$K_D$ bulk distribution coefficient, mL/g.
$K_v$ volumetric distribution coefficient, cm$^3$/cm$^3$.
$K_a$ surface distribution coefficient, cm.
$K_a^s$ surface distribution coefficient determined in sorption step, cm.
$K_a^d$ surface distribution coefficient determined in desorption step, cm.
$M$ activity of tracer injected into resident solution, Bq.
$Pe$ Peclet number, $ux/D_L$.
$Q$ volumetric discharge, mL/hr.
$R_a$ surface retardation factor.
$t$ time, hours.
$t_0$ tracer residence time, hours.
$t_w$ water residence time, hours.
$u$ fluid velocity in fracture, cm/s.

$V$ volume of solution contacting rock coupons, mL.
$V_f$ volume of fracture, mL.
$V_t$ total volume of fracture and tubing, mL.
$x$ distance along the fracture, m.
$z$ distance into rock matrix, m.
$\delta(t)$ Dirac delta function, 1/hr.
$\rho_s$ density of intact rock, including pores, g/cm$^3$.
$\varepsilon_p$ porosity of rock matrix.
$\tau$ tortuosity of the rock matrix.
$\Delta t$ time duration of tracer injection, hour.

**Acknowledgments.** We thank the staff of the Geochemistry Research Branch of AECL's Whiteshell Laboratories for their generous support during this study. Doug Drew provided important technical support, and Kenneth V. Ticknor prepared the autoradiographs. Dana L. Joseph from the Analytical Science Branch performed most of the radiometric analyses. This research has also been supported by a grant from the Natural Science and Engineering Research Council of Canada (NSERC). The review comments of John Kessler, Kent Novakowski, and Todd Rasmussen are appreciated.

## References

Barney, G. S., Radionuclide sorption and desorption reactions with interbed materials from the Columbia River basalt formation, paper presented at 185th American Chemical Society Meeting, Div. of Nucl. Chem. and Tech., Seattle, Wash., 1984.

Brusseau, M. L., and P. S. C. Rao, Sorption non-ideality during organic contaminant transport in porous media, *Crit. Rev. Environ. Control*, *19*(1), 33–99, 1989.

Davis, J. A., and D. B. Kent, Surface complexation modeling in aqueous geochemistry, in *Mineral-Water Interface Geochemistry*, *Rev. Mineral.*, vol. 23, edited by M. F. Hochella and A. F. White, Mineral. Soc. of Am., Washington, D. C., 1990.

Dverstorp, B., J. Andersson, and W. Nordqvist, Discrete fracture network interpretation of field tracer migration in sparsely fractured rock, *Water Resour. Res.*, *28*, 2327–2343, 1992.

Fujikawa, Y., and M. Fukui, Adsorptive solute transport in fractured rock: Analytical solutions for delta-type source conditions, *J. Contam. Hydrol.*, *6*, 85–102, 1990.

Fujikawa, Y., M. Fukui, D. J. Drew, and T. T. Vandergraaf, Analysis of the migration of instantaneously injected cesium in artificial fractures of Lac du Bonnet granite, Manitoba, Canada, *J. Contam. Hydrol.*, *14*, 207–232, 1993.

Hölttä, P., M. Hakanen, and A. Haotojärvi, Migration of radionuclides in fracture columns, in *Scientific Basis for Radioactive Waste Management XIV*, edited by T. Abrajano and L. H. Johnson, pp. 649–656, Mater. Res. Soc., Pittsburgh, Pa., 1991.

Kessler, J. H., and J. R. Hunt, Dissolved and colloidal contaminant transport in a partially clogged fracture, *Water Resour. Res.*, *30*, 1195–1206, 1994.

Kreft, A., and A. Zuber, On the physical meaning of the dispersion equation and its solutions for different initial and boundary conditions, *Chem. Eng. Sci.*, *31*, 1471–1480, 1978.

Maloszweski, P., and A. Zuber, Mathematical modeling of tracer behavior in short-term experiments in fissured rocks, *Water Resour. Res.*, *26*, 1517–1528, 1990.

Moreno, L., and I. Neretnieks, Flow and nuclide transport in fractured media: The importance of the flow-wetted surface for radionuclide migration, *J. Contam. Hydrol.*, *13*, 49–71, 1993.

Moreno, L., I. Neretnieks, and T. Eriksen, Analysis of some laboratory tracer runs in natural fissures, *Water Resour. Res.*, *21*, 951–958, 1985.

Neretnieks, I., Diffusion in the rock matrix: An important factor in radionuclide retardation? *J. Geophys. Res.*, *85*, 4379–4397, 1980.

Neretnieks, I., T. Eriksen, and P. Tähtinen, Tracer movement in a single fissure in granitic rock: Some experimental results and their interpretation, *Water Resour. Res.*, *18*, 849–858, 1982.

Rasmussen, T. C., Laboratory characterization of fluid flow parameters in a porous rock containing a discrete fracture, *Geophys. Res. Lett.*, *22*(11), 1401–1404, 1995.

Skagius, K., G. Svedberg, and I. Neretnieks, A study of strontium and cesium sorption on granite, *Nucl. Technol.*, *59*, 302–313, 1982.

Ticknor, K. V., T. T. Vandergraaf, and D. C. Kamineni, Radionuclide sorption on mineral and rock thin sections, II, Sorption on granitic rock, *Tech. Rep. TR 385*, At. Energy of Can. Ltd., Chalk River, Ont., 1986.

Tompson, A. F. B., Numerical simulation of chemical migration in physically and chemically heterogeneous porous media, *Water Resour. Res.*, *29*, 3709–3726, 1993.

Torstenfelt, B., K. Andersson, and B. Allard, Sorption of strontium and cesium on rocks and minerals, *Chem. Geol.*, *36*, 123–137, 1982.

Vandergraaf, T. T., Radionuclide migration experiments under laboratory conditions, *Geophys. Res. Lett.*, *22*(11), 1409–1412, 1995.

Vandergraaf, T. T., and D. R. M. Abry, Radionuclide sorption on drill core material from the Canadian Shield, *Nucl. Technol.*, *57*, 399–412, 1982.

Vandergraaf, T. T., D. M. Grondin, and D. J. Drew, Laboratory radionuclide migration experiments at a scale of one meter, *Mater. Res. Soc. Symp. Proc.*, *112*, 159–168, 1988.

Vandergraaf, T. T., C.-K. Park, and D. J. Drew, Migration of conservative and poorly-sorbing tracers in granite fractures, paper presented at 5th International Conference on High Level Radioactive Waste Management, Am. Nucl. Soc., Las Vegas, Nev., 1994.

Wels, C., Transport of sorbing solutes in fractured media: A numerical and experimental analysis of dispersion and retardation, Ph.D. thesis, Univ. of B. C., Vancouver, B. C., Canada, 1995.

Wels, C., and L. Smith, Retardation of sorbing solutes in fractured media, *Water Resour. Res.*, *30*, 2547–2563, 1994.

L. Smith, Department of Earth and Ocean Sciences, 6339 Stores Road, University of British Columbia, Vancouver, B. C., Canada, V6T 1Z4.

T. T. Vandergraaf, Whiteshell Laboratories, Atomic Energy of Canada Limited, Pinawa, Manitoba, Canada R0E 1L0.

C. Wels, Robertson Geoconsultants, Inc., 580 Hornby Street, Vancouver, B. C., Canada, V6C 3B6.

(Received August 2, 1995; revised March 6, 1996;
accepted March 20, 1996.)